Multiscale evaluation of potential damage in jetted lateral boreholes

Bakker, Richard R.; Barnhoorn, Auke

DOI
10.1016/j.ijrmms.2019.03.027

Publication date
2019

Document Version
Final published version

Published in
International Journal of Rock Mechanics and Mining Sciences

International Journal of Rock Mechanics and Mining Sciences 121 (2019) 104007

Contents lists available at ScienceDirect

International Journal of Rock Mechanics and Mining Sciences

journal homepage: www.elsevier.com/locate/ijrmms

Multiscale evaluation of potential damage in jetted lateral boreholes

Richard R. Bakker*, Auke Barnhoorn

Delft University of Technology, Faculty of Civil Engineering and Geosciences, Building 23, Stevinweg 1, 2628 CN, Delft, the Netherlands

ARTICLE INFO

Keywords:
Jet drilling
Lateral damage
CT scan analysis
UCS testing
True-triaxial testing
Sample variability

ABSTRACT

We study the potential formation damage effects due to radial jet drilling on Bentheim sandstone, a homogeneous sandstone that is well established in terms of mechanical properties and widely used as reservoir analogue. We quantify how properties degrade with distance from a jetted hole on μm scale (porosity) and cm scale (compressive, tensile and acoustical properties). Moreover, we perform true-triaxial compression tests on samples with and without a jetted hole. It is concluded that, for this material, jetting has no direct influence on the surrounding area. No significant changes compared to intact material is found, nor can a significant change be detected with respect to distance to a jetted hole. Differences fall within the intra-block variability, and differences between blocks can be well explained by block-to-block variation. Differences in results of the true-triaxial compression tests can be attributed to a different sample geometry, which is corroborated by a numerical simulation. We conclude that the stress field around the jetted hole can therefore be well approximated by the Kirsch equations, modified for compression, and thereby accurately describe the stability of the lateral borehole.

1. Introduction

To improve connectivity of subsurface reservoirs to wellbores, stimulation techniques are used.[1] These include chemical,[2] thermal[3,4] and hydraulic methods.[5] A recent additional method is to drill lateral boreholes (i.e., laterals). One emerging technique of drilling such laterals is by means of high pressure water jets, known as radial jet drilling.[6–11] While a significant amount of research is done on the development of the technique itself, little work has focused on assessing the damage around the jetted hole. It is important to verify the long-term stability of the laterals, and thereby overall production efficiency of the well over time. In this work we assess formation damage caused by radial jet drilling by a variety of laboratory and imaging methods, and estimate formation damage on different length scales. We analyze micro-scale damage by analyzing CT scans of cores taken close to a jetted hole. Often damage that cannot be recognized in microstructural analysis can have an effect on acoustic and mechanical properties. We therefore studied changes in acoustic and mechanical properties (Uniaxial Compressive Strength (UCS) and indirect tensile strength) on cores taken some centimeters from a jetted hole. And finally, we assess the elastic properties of a block of 300 × 300 × 300 mm with a jetted hole in place (roughly 25 mm diameter) and compare it to the properties of intact material.

2. Material and methods

2.1. Sampling material and sampling approach

To be able to analyze the effects of jetted holes, we used Bentheim Sandstone, a material that is well characterized in literature.[12–16] All sample material was collected from the same site, and some blocks were jetted in a controlled laboratory environment at ambient conditions at the facilities of Geothermie Zentrum Bochum, Germany. The block was jetted using tap-water and a commercially available rotary type jetting nozzle (Stonage™ Beetle BT18), connected to a high pressure pump (fluid pressure up to 400 bar) with a controlled flow-rate of 20–25 l/min at room temperature.

While the material shows some variation from block to block and might depend on method of choice,[14] our samples showed an initial porosity of 24.0 ± 1.0% as measured by helium pycnometry. Mineralogy was measured using a Bruker D8 Advance diffractometer, and showed the samples consists mostly of quartz grains with minor amounts of Calcite. Bulk rock density was measured at 2.010 ± 0.015 kg/m^3.

Intact rock material is compared to jetted material in three different types of analysis on different length scales, each requiring different sampling methods. For 3D microstructural analysis (μm scale) we studied cores (10 mm in diameter, approximately 90 mm long) drilled towards the jetted hole wall (see Fig. 1, "μCT cores"). These cores were

* Corresponding author.
E-mail address: r.r.bakker@tudelft.nl (R.R. Bakker).

https://doi.org/10.1016/j.ijrmms.2019.03.027
Received 16 October 2018; Received in revised form 12 March 2019; Accepted 18 March 2019

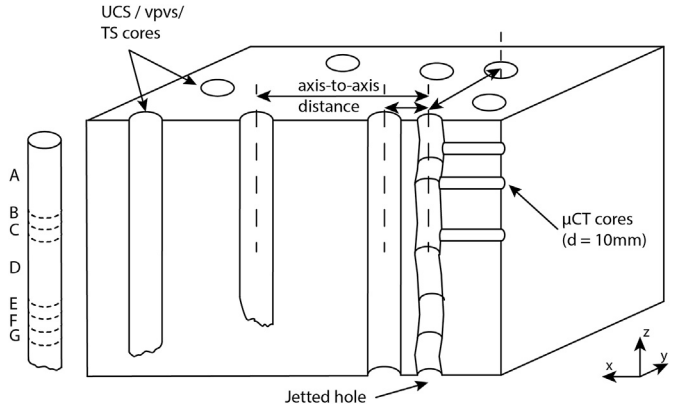

Fig. 1. Schematic overview of the sub-sampling routine for the various tests.

drilled in x direction, with the jetted hole drilled in the *z* direction.

Samples for acoustic testing, UCS, indirect tensile strength testing were obtained from cores that were drilled parallel to the jetted hole (i.e., z-direction), varying the axis-to-axis distance on a cm-scale (see Fig. 1, "UCS/vpvs/TS cores"). In total, fourteen cores of 30 mm in diameter were drilled with axis-to-axis distances varying from 30 to 100 mm. Note that the jet-hole itself had a diameter of approximately 20 mm, and therefore the minimum axis-to-axis distance was 30 mm, ensuring the cores would be full cylinders. The total length of the cores varied between 180 and 240 mm. Each core was subdivided (cut with a diamond blade saw) to yield cores labelled A-G in Fig. 1, suitable for non-destructive acoustic tests, UCS tests and indirect tensile strength testing (i.e., Brazil disk method). Of each core 2 samples of approximately 75 mm length were prepared for compressive tests, according to a standard 2.5-1 length to diameter ratio.[17] The rest of the available core length was used to make disks of approximately 15 mm length, for Brazil Disk indirect tensile strength measurements, and fracture toughness[18] with a minimum of two samples per core. Samples were labelled according to core number and relative axial location within the core (Fig. 1, left side).

Finally, to assess the bulk rock properties with and without a jetted hole, conventional tri-axial testing could not be used due to the dimensions of the provided jetted holes compared to sample size. We therefore use a true-triaxial apparatus capable of handling large samples: cubic samples of 300 mm × 300 mm × 300 mm. Tests were performed on an intact block, and on a second block with a jetted hole running from the center of one cube-face towards the opposing side, along the central *y*-axis. The jetted borehole was created using the same conditions as described above.

2.2. Micrometer scale analysis

Three cores with a diameter of 10 mm were analyzed using a Phoenix Nanotom - microCT Computed Tomography System as installed at the laboratory of TU Delft. The achieved resolution of the scan depends on the sample size, here the voxel size was 5.5 μm. To detect changes along the core direction (i.e., varying distance to the jet hole) we also analyzed the porosity changes automatically: consecutive 2D slices of the reconstructed volume were analyzed using a scripted image analysis routine. This routine first omits pixels that are considered outside of the sample (yellow line in Fig. 2A) and subsequently uses the remaining pixels to calculate the gray-scale value distribution (histogram). From this histogram two peaks emerge, which are associated with either "pore" (both primary and secondary) or "grain" phases. The grayscale value that is associated with the local minimum between the two peaks is taken as the threshold between the two phases, and is used to calculate fraction between the two, which is the 2D thresholded porosity; (see Fig. 2B, threshold grayscale value in this for the image shown in A would be around 0.08). With consecutive CT scan slices this results in a micrometer-scale resolution porosity profile. We focused on image-slices closest to the jet-hole, as well as a few cm away from the jet-hole wall for comparison.

2.3. Centimeter scale: core tests

2.3.1. Acoustic wave speeds

Rock samples that were prepared for uniaxial strength testing were first used for non-destructive acoustic wave speeds measurements. Acoustic transducers with peak sensitivity of 1 MHz were placed directly on the end-faces of the cylindrical samples, with coupling gel in between, ensuring a good signal transfer. A single pulse of 1 MHz was applied to the transmitter, and picked up by the receiver, which in turn was connected to a high-speed acquisition oscilloscope (type: Yokogawa DLM4000). This procedure was repeated at least 1000× to obtain an average signal, limiting the effect of noise. We used both p-wave transducers (type: Panametrics, V103-RM), and s-wave transducers (type: Panametrics V153-RM). Arrival times were determined by analyzing the stored waveform in post processing, analyzing both the waveform itself, as well as the spectrogram. The latter was primarily used for determining s-wave arrival, due to scattering of the p-wave that arrived earlier.

2.3.2. Uniaxial compressive strength tests

Static elastic properties and mechanical strength in compression was tested using a stiff in-house built deformation apparatus, capable of handling load up to 500 kN. All samples were deformed at a constant displacement rate, such that the resulting engineering strain rate was 10^{-5} s^{-1}, while measuring the resulting load. Axial displacement was measured continuously by two LVDTs. Radial displacement was measured by a chain-type LVDT (model MTS 815). All data was logged at 2 Hz to ensure sufficient data points for post processing, as well as capture peak stress adequately. Elastic properties were determined by evaluating the stress-strain curves, correcting for sample assembly settling and crack closure at the initial part of the curve, and crack formation effects when close to macroscopic failure (final part of the curve). The linear part of the loading curve (between approximately 30 to 70% of maximum axial stress) was used, fitting the data against axial and radial strain with a first-order polynomial. The slope of the fit with axial strain is used as the Young's modulus, and the Poisson's ratio is determined by dividing the slope of the axial stress vs axial strain over axial stress vs radial strain. Using this approach, we additionally determine the error of fit and thereby yield errors of the elastic properties for each specimen.

2.3.3. Tensile properties (tensile strength and fracture toughness)

Tensile strength and fracture toughness were determined using the (modified) Brazil disk method.[18] Tests were performed in an in-house built deformation apparatus, capable of handling axial load up to 50 kN, measured by a high-precision load cell (0.01 kN resolution). Displacement was measured by two LVDT's mounted parallel to the loading direction. A constant displacement rate of 0.8 μm/s was imposed such that failure would occur within a few minutes, which was determined by a calibration run in ramp-load mode. Data was logged at 10 Hz, such that the peak load could precisely be determined in post processing.

2.4. Decimeter scale: true triaxial testing

To assess how elastic properties of the material is affected by a jetted borehole and potential damage zone, a large sample is needed, as the jetted borehole has a diameter of approximately 3 cm and the size of the potential damage zone is unknown. To test such a large sample would avoid any potential damage caused by sub-sampling as described in the methods above. To test a large block (300 × 300 × 300 mm), we

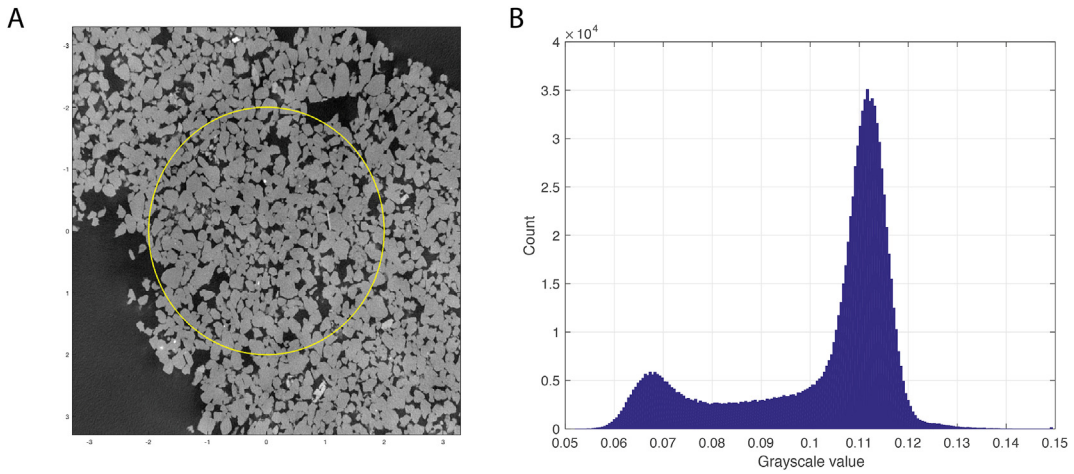

Fig. 2. A) example µCT scan image slice, B) example of the associated histogram.

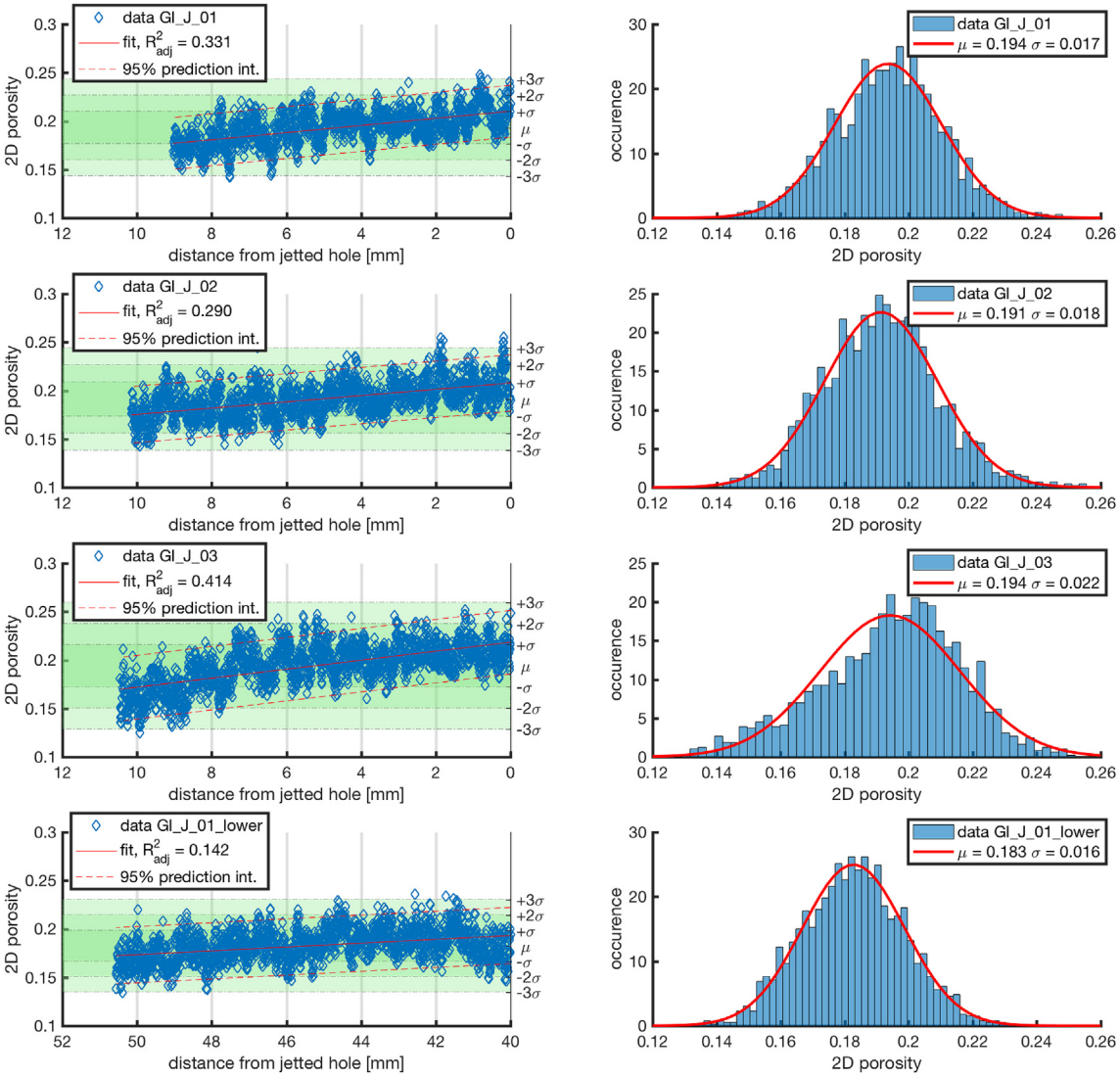

Fig. 3. CT scan based porosity variation for 3 cores close to the borehole wall (0 to approx. 12 mm, samples GI_J_01, GI_J_02 and GI_J_03) and one further away from the borehole (~40–50 mm).

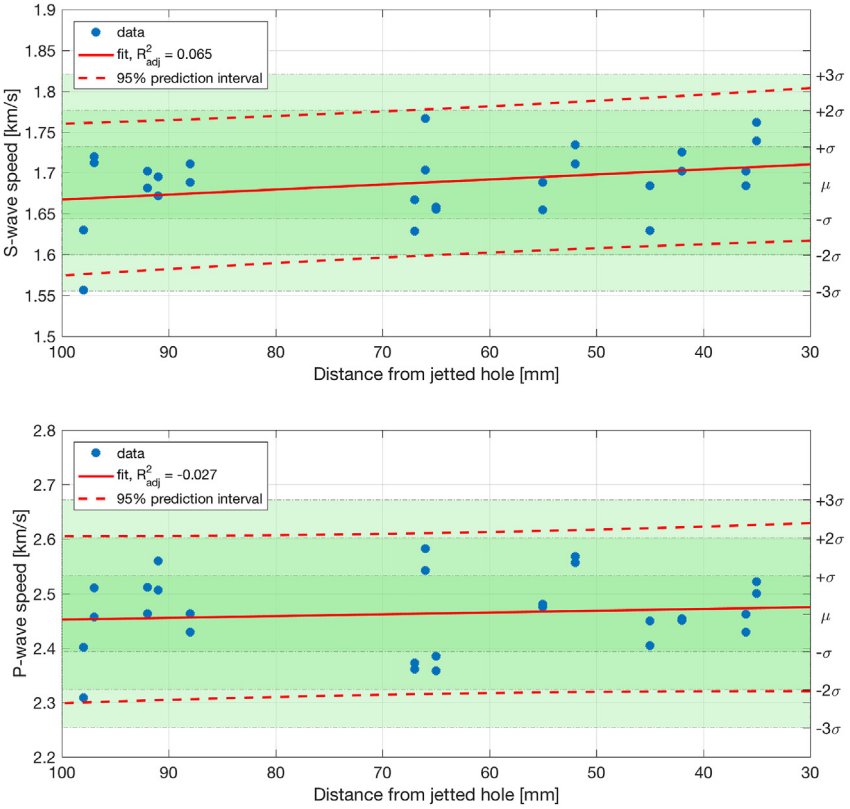

Fig. 4. Acoustic wave speeds of samples, taken at a certain distance from a jetted hole (axis-to-axis). Upper diagram: s-wave speeds. Lower diagram: p-wave speeds.

use the true-triaxial deformation apparatus as installed in the TU Delft rock mechanics laboratory.[19,20] This apparatus is able to handle large cubical samples with independently-controlled loads up to 350 tons (~3430 kN), in three orthogonal directions (*x, y, z*). For these experiments this results in a maximum stress of 38.1 MPa. The experiment was conducted in four phases, all starting from a hydrostatic state of stress of 3 MPa. Similar to the UCS experiments, this load was chosen to avoid inelastic effects due to machine settling etc. During the entire run the displacement between two opposing sample faces was measured by two LVDTs per direction. In the first phase the samples were loaded hydrostatically, such that the resulting displacement measurement lead to at least 0.1% strain in all directions. Since the apparatus operates in load control mode, in practice this meant loading the block up to 30 MPa. Thereby the stress-strain curve has sufficient resolution to determine elastic properties, which is done with the same regression technique as with the UCS tests described above.

In the second phase the load in y and z directions was kept constant at 3 MPa, while the load in the *x* direction was increased to result in at least 0.1% coaxial strain (similarly to phase 1, albeit to 20 MPa as less stress is required to strain the sample in non-hydrostatic deformation). By keeping the load in lateral directions (*y,z*) constant, the pistons in the *y* and *z* directions would move outward to cope with increased load due to lateral expansion, and thereby the lateral expansion is measured. The third and fourth phases were similar to phase 2, but with different stress orientations (load in *y*, or *z* direction). With a known UCS strength of 40–50 MPa for Bentheim sandstone[14] we ensure that our samples do not exceed the elastic domain in terms of stress. We therefore assume that the sample did not acquire additional (micro-) crack damage during the loading procedure. Data was logged with a frequency of 1 Hz.

3. Results

3.1. Porosity analysis based on μCT

Porosity (fraction) measured by this method varied strongly between 0.12 and 0.26. As depicted in Fig. 3, the jet hole wall is on the right hand side of the diagram (at 0 mm). For each of the four samples the diagram on the left side shows the porosity for each slice. For samples GI_J_01, GI_J_02 and GI_J_03, a linear fit was attempted on (0–10 mm from jet hole wall) to determine the change in porosity towards the jetted hole. Considering that the $r^2_{adjusted}$ (coefficient of determination) value is the fraction by which the variance of the regression-errors is less than the variance of the data, corrected for the number of parameters that were used in the fitting, low values represent that the variance of the regression-errors and the variance the data itself are close. That implies the regression is qualitatively only marginally better than a random normal distribution at describing systematical changes in data. Therefore, given the low $r^2_{adjusted}$ values as well as the broad prediction interval, we cannot distinguish with statistical certainty that there are changes in porosity with respect to distance to the jet hole wall, in either of the three cores.

Despite this caveat, (that the linear fits are not that robust compared to a random distribution) in all cases, a small general towards higher porosities close to the jetted hole wall is detected (~3% porosity increase). For consistency (and cross-validation) the lower part of core 01 was also checked for porosity changes along axis using the same scanning-settings. While this sample was taken from the same drilled core, at > 40 mm away from the jet hole wall we consider the material unaffected by jetting. Here a similar general upward trend in porosity, with similar change in magnitude was observed, as well as with relatively large uncertainty depicted by the broad prediction interval (Fig. 3, sample GI_J_01_lower).

Moreover, when we compare the results from the jetted and unjetted cores, we see similar trends. Considering the samples on average

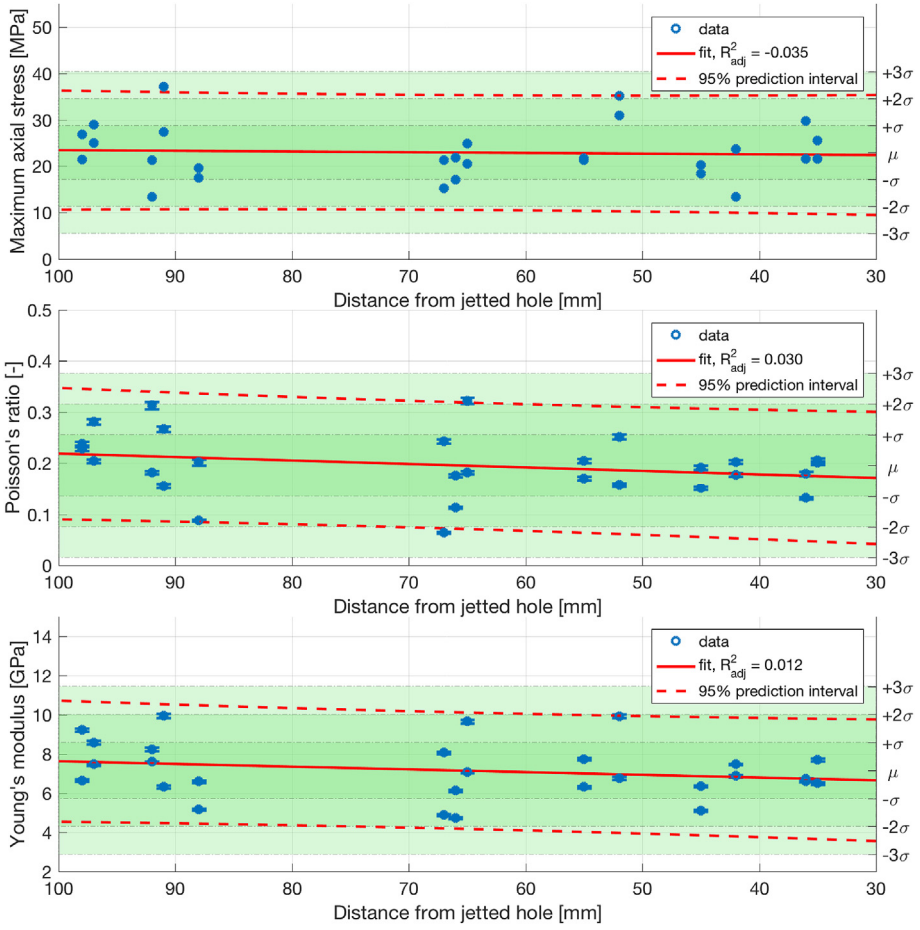

Fig. 5. Results of UCS tests at various distance of jetted hole. Upper diagram: peak stress at failure. Middle diagram: Poisson's ratio. Lower diagram: Young's moduli.

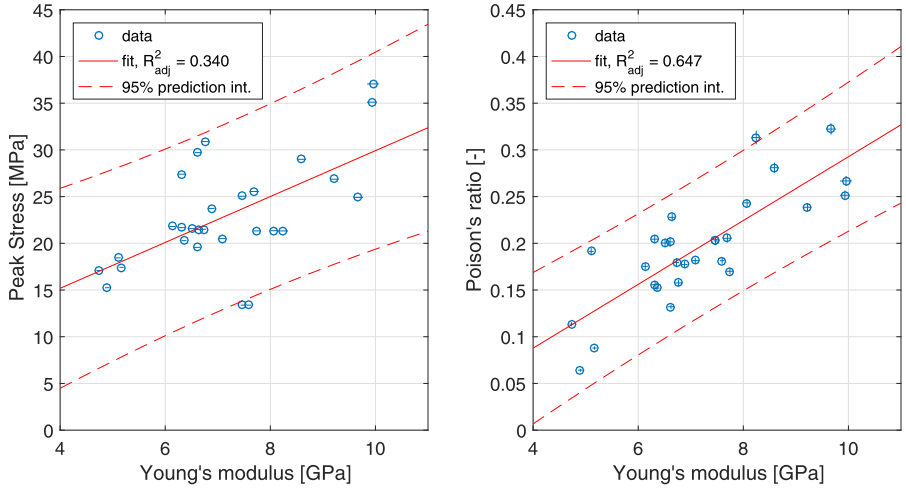

Fig. 6. Cross plots for uniaxial compression data. Left diagram: Peak stress vs Young's Modulus. Right diagram: Poisson's ratio vs Young's modulus.

(when trends are not considered and the porosity distribution data depicted on the right of Fig. 3) they show similar variability in porosity values, and equally large standard deviations (visible by the width of the Gaussian curves). Because the absolute differences between measured average porosity fall within the standard deviation for all cores, we do not consider the differences between cores to be significant.

3.2. Acoustic properties with distance from jetted hole

We find a general increase in acoustic wave speeds towards the jetted hole wall (see Fig. 4, the distance from the jetted hole decreases from left to right, measurement errors are smaller than the depicted symbol size). However, coefficients of determination ($r^2_{adjusted}$-values) are too low to consider these statistically meaningful (0.065 for v_s, -0.027 for v_p). Indeed, negative $r^2_{adjusted}$-values indicate that the independent variables have too little predictive value. Accordingly, no significant changes in acoustic wave speeds with respect to distance to the jetted hole could be detected. Overall measured values range between 2.3 and 2.6 km/s (v_p) and 1.6–1.8 km/s (v_s, Fig. 4). These are consistent with that of unjetted material (v_p = 2.61 km/s and

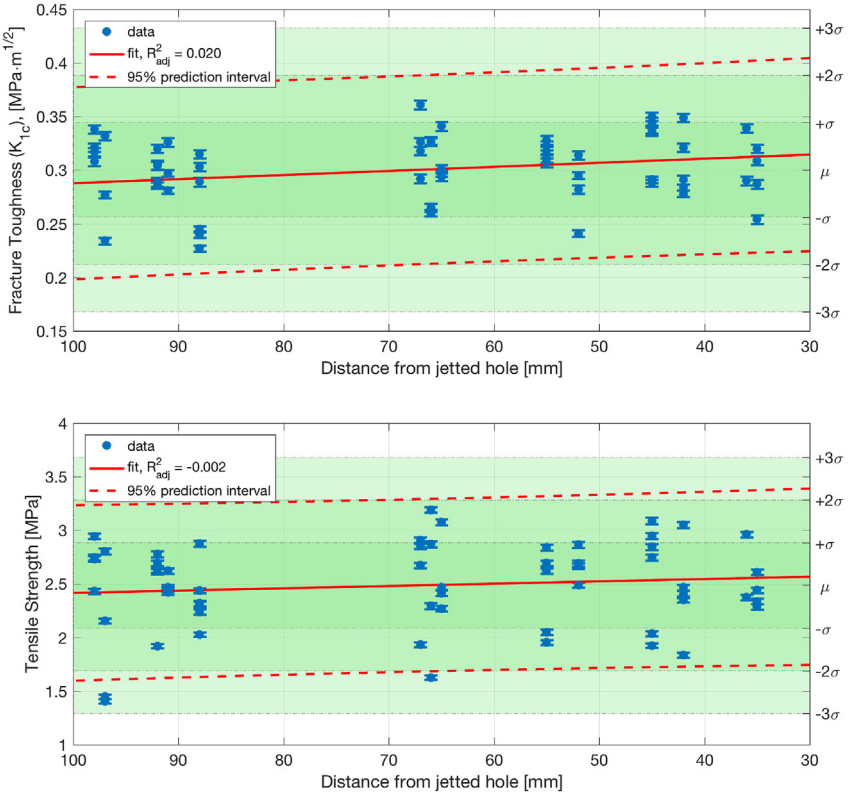

Fig. 7. Results of tensile tests on cores obtained at various distance of jetted hole. Upper diagram: fracture toughness. Lower diagram: tensile strength.

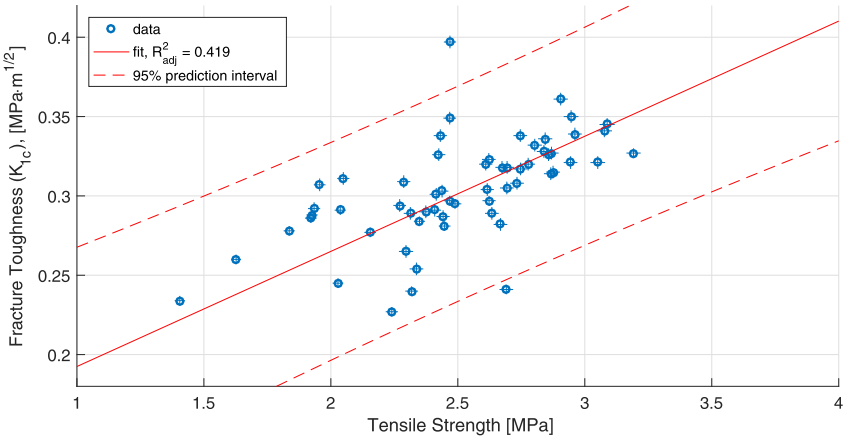

Fig. 8. Cross plot for tensile properties, showing a general correlation between Fracture Toughness and Tensile Strength.

v_s = 1.75 km/s, note that these are measured on a different block originating from the same quarry).

3.3. Uniaxial compressive strength with distance to jetted hole

Overall trends revealed no obvious tendency in measured maximum axial stress towards the jetted hole. Ultimate failure strength results range between 13 and 38 MPa. Slight decreases in elastic properties could be observed, but similar to the acoustic wave speed measurements, these changes are not statistically meaningful. Therefore, no changes in elastic properties, nor ultimate failure strength with respect to distance to the jetted hole was found (Fig. 5, for all diagrams the distance from the jetted hole decreases from left to right.). Elastic properties were found to be variable, with Young's Modulus found to range between 5 and 11 GPa and Poisson's ratios between 0.06 and 0.32, with stiff samples generally having a higher Poisson's ratio (Fig. 6). There is a similar correlation (although less well constraint) between ultimate strength and elastic properties (Fig. 6), with stiffer samples having a higher ultimate failure strength.

3.4. Fracture toughness and tensile strength with distance to jetted hole

Counter intuitive, slight upward trends in tensile properties (fracture toughness and tensile strength) towards the jetted hole could be detected. However, again these trends are not statistically significant with adjusted r^2-values of 0.020 for fracture toughness and -0.002 for tensile strength (see Fig. 7, the distance from the jetted hole decreases from left to right.). Fracture toughness (K_{1c}) values range between 0.22 and 0.44 MPa m$^{1/2}$. Tensile strength values range between 1.4 and 3.2 MPa. Similar to the UCS test results, a qualitative relation between tensile strength and fracture toughness emerges from the data, with higher tensile strength associated with high values in fracture

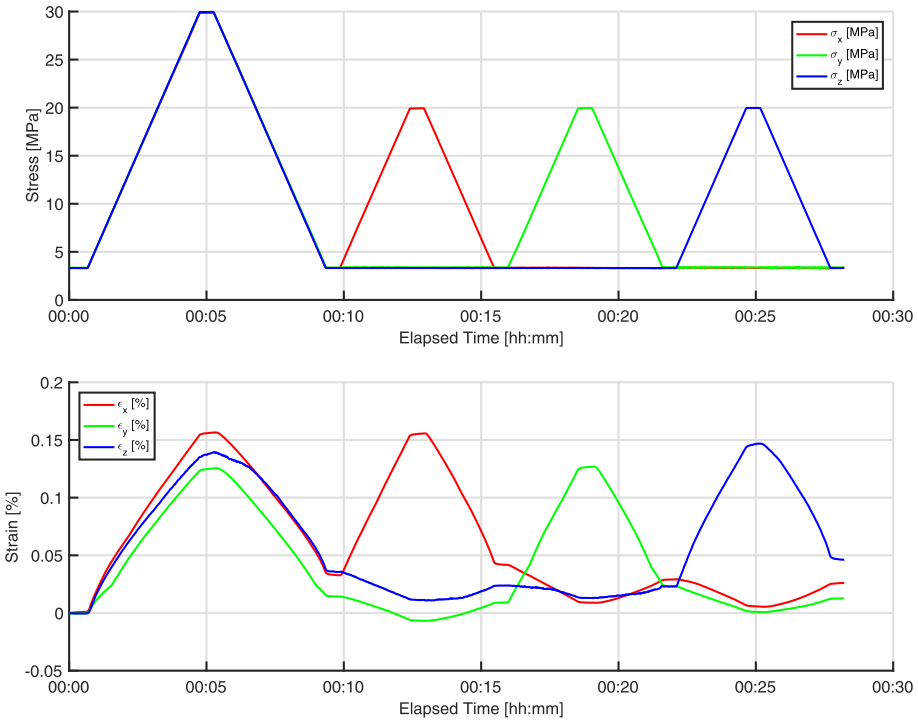

Fig. 9. Example of a true-triaxial test on a block with a jetted hole borehole. Upper diagram: applied load (x,y,z) vs time. Lower diagram: resulting strain (x,y,z) vs time.

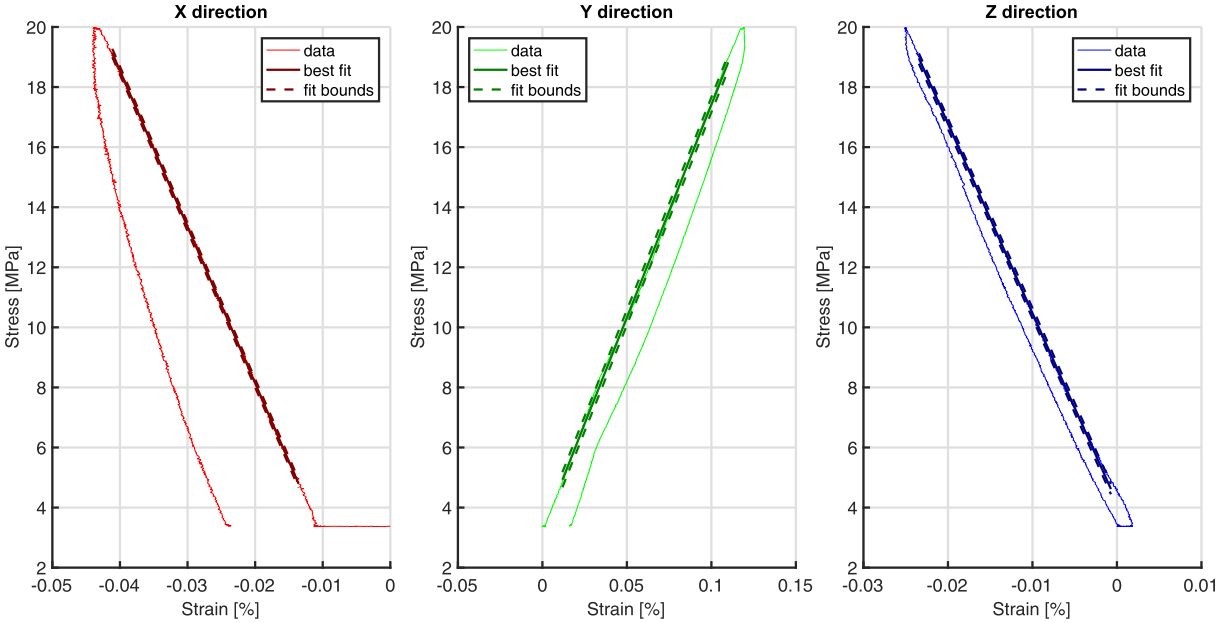

Fig. 10. Example of determination of elastic properties, with load applied in y-direction (same as the axis of the jetted hole). X and Z-directions show lateral expansion as result of the applied stress in y direction.

toughness and vice versa (see Fig. 8).

3.5. Comparing intact material with jetted in true-triaxial testing

Both intact and jetted blocks were subjected to the same loading phases, as indicated by the stress/time and strain/time graphs, shown in Fig. 9. For each phase, the elastic properties were determined form the stress-strain graphs (example is shown in Fig. 10). As can be seen in Fig. 10, the response in the unloading phase was not perfectly elastic, as some non-linear effects are observed. For this reason, only the loading part of stress-strain graphs was used to determine the elastic properties. For jetted blocks, the elastic properties are that of an irregular shape, and do not necessarily reflect the material's true properties. We therefore denote these as apparent elastic properties.

Differences in measured (apparent) elastic response during all phases is plotted in Fig. 13. In the cases “jetted” and “modelled” the jetted borehole runs along the *y* axis in the middle of the block. Different colors indicate directions (RGB = *xyz*). The first dataset is depicted in regular RGB colors and represents the mechanical test on intact material. Darker colors correspond to the second dataset: mechanical test on a jetted block (“jetted”). Finally, the third dataset, depicted in lighter colors correspond to the results of a numerical model

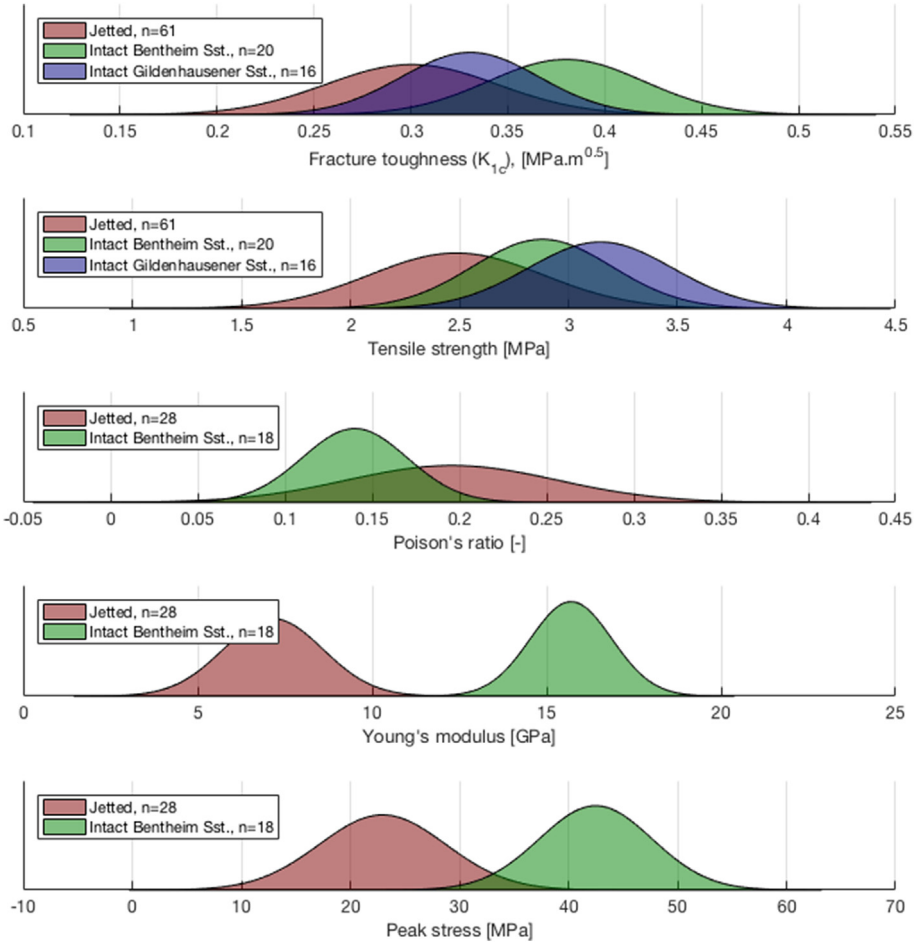

Fig. 11. Gaussian distributions based on averages and standard deviations for intact rocks compared to Jetted material.

("modelled"). Note that shortening is taken positive, thereby the negative values shown in the lower part of Fig. 13 imply lateral (orthogonal) expansion as a response to an axial load. In terms of strain magnitude, this expansion is considerably less compared to co-axial strain. However, as the expansion coefficient is defined as the slope of axial stress to the strain in a particular orthogonal direction, this result in considerably higher magnitudes. These values are depicted in the lower diagram of Fig. 13, and are used to calculate the (apparent) Poisson's ratios that are shown in the upper diagram.

We did not find notable changes in hydrostatic compaction of the blocks (first phase). For applied load in a single direction (i.e., stages 2, 3 and 4) some differences could be observed that are likely beyond that which can be explained by intra-sample variation. These differences are mainly in the lateral response to the applied load (i.e., Poisson's ratios, Fig. 13). With a jetted hole in place the lateral expansion is less compared to intact material by a factor of roughly 1.5, as shown by the stiffer elastic responses (higher moduli). Possibly some of the strain could be accounted for by deformation (shrinking) of the jetted hole itself, but this could not be adequately measured due to the irregular shape of the jetted hole.

4. Discussion

From the μCT-analysis, all samples seem to show an increase of porosity towards the jetted wall, that includes a lower part that was some 40 mm away from the jetted wall. If a trend may be inferred, the porosity increases with ~0.4% per mm, but these data cannot be extrapolated beyond the regression interval with certainty. The increase is not statistically significant based on the poor fit (see various adjusted r^2-values, Fig. 3) and could be due to a calculation artefact in the reconstruction of the raw-images to a 3D volume, or a non-equal response of the CT-scan detector. Moreover, when comparing histograms for the 2D porosity data (plotted on equal horizontal axis), it is evident that the normal distributions overlap, and cannot be statistically distinguished from each other.

Porosity averages are slightly lower compared to those measured by helium pycnometry on in-tact material, which falls in the range of 23.4–25.1%. The discrepancy can be explained by pores that are too small to be imaged by μCT analysis,[14,21] as well as grain geometries that are not sufficiently sampled by the scan resolution.[22,23] However, for our purpose we compare 2D slices with the exact same resolution directly with one another. All images in that stack are affected equally by the discrepancy between "CT-porosity" and that measured by helium pycnometry, thus the relative changes within the 2D-porosity with distance from the jetted borehole wall may still be identified. Moreover, sub-sampling to allow for helium-pycnometry on smaller samples compared to the 10 mm diameter cores is impractical, as drilling cores with < 10 mm diameters could potentially induce fractures by drilling the sub-samples, and samples are likely not perfect right-cylinders to allow accurate pycnometry.

From the cores drilled adjacent to the jetted hole (varying distance), no significant trends either of the following: acoustic wave speeds (both v_p & v_s); elastic properties in compression, ultimate failure strength; tensile strength; and fracture toughness. Assuming there is no trend with distance to the jetted hole, all data can be averaged and the intra-block variation can be determined, given there are enough samples. This variation may be best described by the standard deviation of the data. If we then compare with intact material, we can see that the intra-

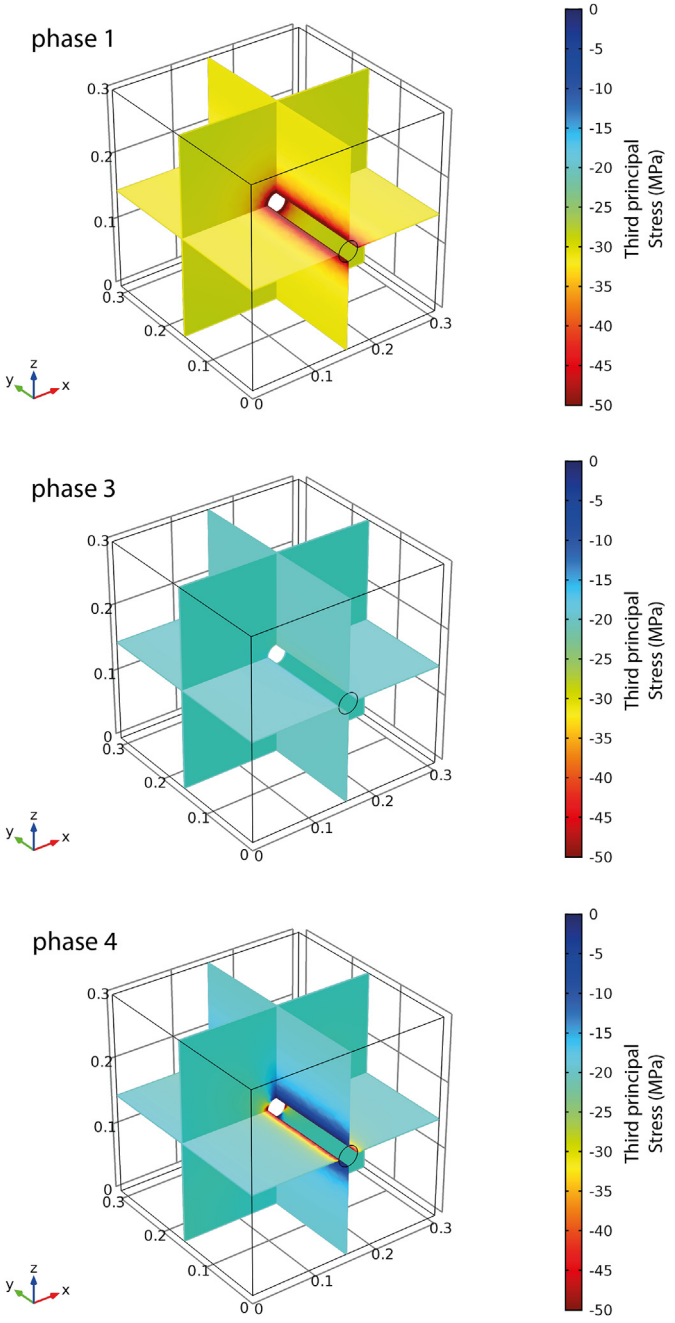

Fig. 12. Example results of the finite element model runs, simulating the true-triaxial experiment in phases: 1 (x/y/z = 30 MPa), 3 (x/y/z = 3/20/3 MPa) and 4 (x/y/z = 3/3/20 MPa).

block variability is similar for most properties (i.e., the width of the Gaussian curves in Fig. 11). Meter-scale variation from block to block (i.e., centers of Gaussian curves) can still exist due to slight differences in rock-type, for example as a result of different burial history. Note that Gildehaus and Bentheim samples are essentially the same rock type (same formation) but acquired from different parts within the same quarry.

Overall measured acoustic wave speeds of jetted samples are slightly lower than that of intact material (v_p = 2.61 km/s and v_s = 1.75 km/s), which we interpret to be due to block-to-block variation, similar to the differences observed in elastic (compressive) and tensile properties, as there is no statistical evidence to suggest jetting is the cause of a lower acoustic wave speeds, at least on a scale of 100 mm.

This variability might also explain a part of the differences observed in the true-triaxial tests, but there the results are too big to be explained by normal variability alone. The bulk sample response to the applied loads is particularly different when looking at the Poisson's ratios. Note that for samples with non-regular geometries it is more appropriate to speak of apparent Poisson's ratios. The differences between the responses in lateral expansion can be explained by the fact that the overall geometry of the sample that is being deformed is different.[24–26] Indeed, as shown in Ref. 26, the presence of an (co-axial) borehole in a cylindrical sample leads to lower apparent Poisson's ratios. To see if the different response of the jetted sample compared to the intact sample could be explained by the different geometry alone the tests were simulated using a commercially available finite element software (COMSOL Multiphysics ®). Here, the sample material was modelled as a homogeneous linear elastic medium characterized by a Young's modulus of 15 GPa and a Poisson's ratio of 0.20. The geometry consisted of a cubic block with a central borehole of 2 cm diameter along the *y* axis. The test was simulated by applying the same load path and boundary conditions as the laboratory tests. Fig. 12 shows an example of the stress distribution around the simulated borehole for the first, third and fourth phase of the experiment. In these model runs the engineering stress/strain sign convention is used, whereby negative numbers represent compressive states, thus the third principal stress component represents the maximum compressive stress. To allow for direct comparison, the same color-scale is used for each panel. Note the stress distribution around the circular borehole, particularly in stage 4. The bulk-rock responses in terms of apparent elastic parameters are plotted in Fig. 13. These show a remarkable good match with the measured laboratory data. The numerical results may also be derived using analytical solutions: the standard Kirsch equations describing the stress field around a cylindrical borehole in an external stress field.[27,28] As the simulation and lab data on the jetted borehole give similar results, we therefore argue that the stress field around a jetted borehole may be adequately captured by the Kirsch equations as well, at least for our sample scale (300 mm). However, a more detailed and/or sophisticated numerical approaches can be part of future research to address the stress field in more detail, on a smaller scale.

Although our results show no significant formation damage, we remark that this does not necessarily have to be the case for samples that are jetted while under reservoir conditions (i.e., stress, temperature, pore fluid pressure). However, side-wall samples of in-situ jetted reservoir sections are hard to obtain and are not available as far as the authors are aware at the time of writing this manuscript. Therefore, samples jetted under ambient conditions are by far the best alternative, as sub-sampling blocks jetted at surface conditions is less expensive and allows for more precise (controlled) sampling. Moreover, in this study we have focused on Bentheim Sandstone, which, with a permeability in the order of 1–3 × 10^{-12} m^2 [14] is a rock type where normally such stimulation techniques are not required. However, as this rock has a relatively low UCS and low tensile strength, if radial jet drilling would cause any significant formation damage, it would have been observed in our data, and this might not have been the case for stronger lithologies.

Finally, the jetted samples in our study all had more or less cylindrical boreholes, as samples were drilled with rotary nozzle types. These were chosen as they generally produce better results in the field.[11] Static nozzle types could potentially produce different jet-hole geometries which are potentially less stable than the cylindrical shape.

In this work we set out to find out if there is damage around a jetted borehole, and found no significant changes. However, there are important implications for the long term stability of jetted laterals: assuming jetting boreholes under reservoir conditions results in a cylindrical borehole (similar to surface conditions), and given that rock properties do not significantly degrade around the borehole, jetted boreholes have a good change of remaining stable (open) at reservoir conditions. If the local stresses around the jetted borehole (which can be determined using the Kirsch-equations) are not likely to lead to

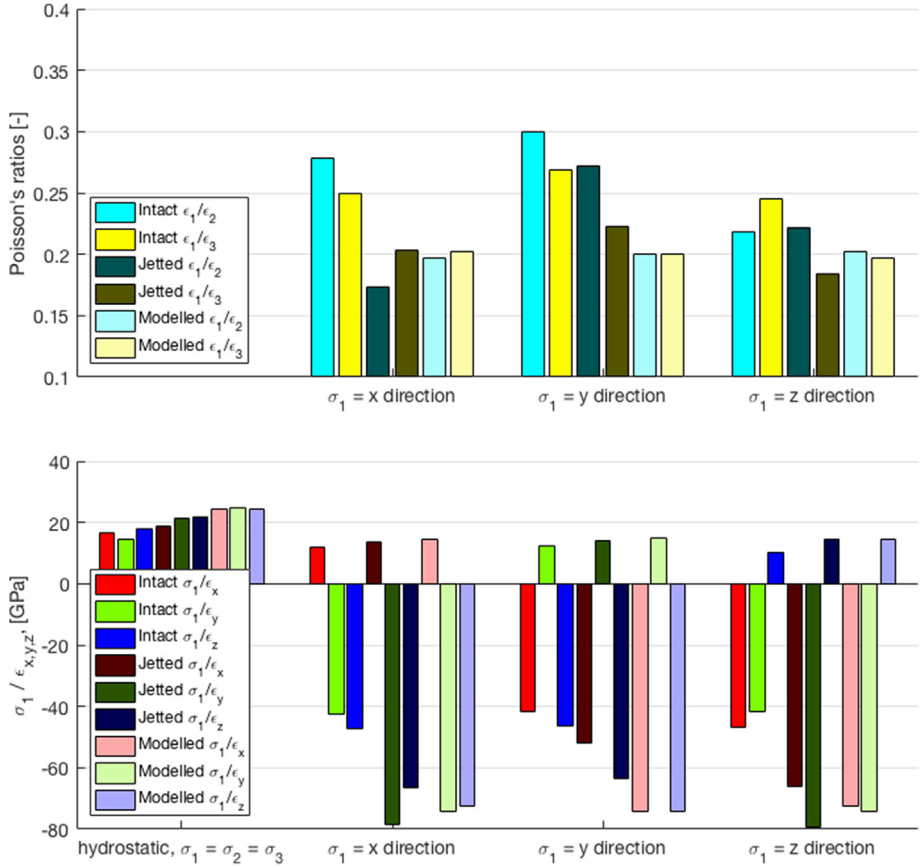

Fig. 13. Overview of resulting elastic properties from three data sets, grouped by experiment stage.

collapse, jetting lateral boreholes may be a valuable long-term investment leading to an overall increased productivity.

5. Conclusion

The near wellbore damage caused by radial jet drilling was assessed on three length scales using various methods. Micrometer scale damage was assessed using CT scans at a voxel resolution of ~5 μm, on a core taken radially outward from the jetted hole. No statistically significant changes in porosity (i.e., secondary porosity or fractures) were observed with increasing proximity to the jet hole.

Centimeter scale damage was assessed using core samples taken with axis parallel to the jet hole direction, varying proximity to the jet hole. No significant changes in acoustic wave speed (v_p, v_s), uniaxial compressive strength, elastic properties, tensile strength or fracture toughness could be detected. When all data is combined to calculate a Gaussian distribution of the properties, it is evident that the intra-block variation is similar to that of intact material. However, averages may vary from block to block according to expected intra-reservoir variation.

Decimeter scale (or bulk rock) damage was measured by subjecting cubic rock samples (one intact, one with jet hole in place) to a true-triaxial stress path while measuring the strain response in three orthogonal directions. Results displayed that the emplacement of the jet hole has had an impact on the elastic properties. Using a numerical simulation (3D, FEM, elastic) we ascertain that this can be attributed purely to stress concentrations around the borehole, due to the different geometry of the sample.

Finally, we conclude that radial jet drilling causes no significant damage in close proximity, and that the stress field around the jet hole can be adequately captured by classical Kirsch equations.

Acknowledgements

This work is funded within the EU Horizon 2020 research and innovation programme under grant agreement No. 654662 (named "SURE"). The authors thank the technical staff of the TU Delft Rock Mechanics laboratory (particularly Marc Friebel, Karel Heller and Jens van der Berg), and Ryan Chhanai for their help. Simon Hahn at Geothermie Zentrum Bochum (Germany) is thanked for providing sampling material (both intact and with jetted laterals). Ruud Hendrikx at the Department of Materials Science and Engineering at TU Delft is acknowledged for X-ray analysis. Finally, we acknowledge the SURE project consortium for discussion of intermediate results.

Appendix A. Supplementary data

Supplementary (raw) data to this article can be found online at https://doi.org/10.4121/uuid:e6fec088-761a-4984-a66c-b544e1172965.

References

1. Huenges E. *Enhanced Geothermal Systems: Review and Status of Research and Development.* Elsevier Ltd; 2016https://doi.org/10.1016/B978-0-08-100337-4.00025-5.
2. Portier S, Vuataz FD, Nami P, Sanjuan B, Gérard A. Chemical stimulation techniques for geothermal wells: experiments on the three-well EGS system at Soultz-sous-Forêts, France. *Geothermics.* 2009;38(4):349–359. https://doi.org/10.1016/j.geothermics.2009.07.001.
3. Kant MA, Rossi E, Duss J, Amann F, Saar MO, Rudolf von Rohr P. Demonstration of thermal borehole enlargement to facilitate controlled reservoir engineering for deep geothermal, oil or gas systems. *Appl Energy.* 2018;212(October 2017):1501–1509. https://doi.org/10.1016/j.apenergy.2018.01.009.
4. Bradford J, McLennan J, Moore J, Podgorney R, Plummer M, Nash G. Analysis of the thermal and hydraulic stimulation program at raft river, Idaho. *Rock Mech Rock Eng.* 2017;50(5):1279–1287. https://doi.org/10.1007/s00603-016-1156-0.

5. Reinicke A, Rybacki E, Stanchits S, Huenges E, Dresen G. Hydraulic fracturing stimulation techniques and formation damage mechanisms-Implications from laboratory testing of tight sandstone-proppant systems. *Chem Erde.* 2010;70(SUPPL. 3):107–117. https://doi.org/10.1016/j.chemer.2010.05.016.
6. Song X, Lyu Z, Cui L, Li G, Ji G, Pang Z. Comparison of numerical analysis on the downhole flow field for multi-orifice hydrothermal jet drilling technology for geothermal wells. *Geothermics.* 2017;70(July):314–323. https://doi.org/10.1016/j.geothermics.2017.07.004.
7. Li J, Li G, Huang Z, Song X, Yang R, Peng K. The self-propelled force model of a multi-orifice nozzle for radial jet drilling. *J Nat Gas Sci Eng.* 2015;24:441–448. https://doi.org/10.1016/j.jngse.2015.04.009.
8. Buset P, Riiber M, Eek A. Jet drilling tool: cost-effective lateral drilling technology for enhanced oil recovery. *Proc SPE/ICoTA Coiled Tubing Roundtable.* 2001:1–9. https://doi.org/10.2523/68504-MS.
9. Dickinson W, Dickinson RW. Horizontal radial drilling system. *SPE Calif Reg Meet.* 1985:887–892. https://doi.org/10.2118/13949-MS.
10. Blöcher G, Peters E, Reinsch T, Petrauskas S, Valickas R, van der Berg S. *D3.2 Report on Radial Jet-Drilling (RJD) Stimulation Technology*. 2016; 2016http://doi.org/10.2312/GFZ.6.2.2018.001.
11. Reinsch T, Paap B, Hahn S, Wittig V, van den Berg S. Insights into the radial water jet drilling technology – application in a quarry. *J Rock Mech Geotech Eng.* 2018:1–13. https://doi.org/10.1016/J.JRMGE.2018.02.001.
12. Klein E, Baud P, Reuschlé T, Wong TF. Mechanical behaviour and failure mode of Bentheim sandstone under triaxial compression. *Phys Chem Earth, Part A Solid Earth Geod.* 2001;26(1-2):21–25. https://doi.org/10.1016/S1464-1895(01)00017-5.
13. Vajdova V, Baud P, Wong TF. Permeability evolution during localized deformation in Bentheim sandstone. *J Geophys Res B Solid Earth.* 2004;109(10):1–15. https://doi.org/10.1029/2003JB002942.
14. Peksa AE, Wolf KHAA, Zitha PLJ. Bentheimer sandstone revisited for experimental purposes. *Mar Petrol Geol.* 2015;67:701–719. https://doi.org/10.1016/j.marpetgeo.2015.06.001.
15. Benson PM, Meredith PG, Platzman ES, White RE. Pore fabric shape anisotropy in porous sandstones and its relation to elastic wave velocity and permeability anisotropy under hydrostatic pressure. *Int J Rock Mech Min Sci.* 2005;42(7-8 SPEC. ISS.):890–899. https://doi.org/10.1016/j.ijrmms.2005.05.003.
16. Dautriat J, Gland N, Guelard J, Dimanov A, Raphanel JL. Axial and radial permeability evolutions of compressed sandstones: end effects and shear-band induced permeability anisotropy. *Pure Appl Geophys.* 2009;166(5-7):1037–1061. https://doi.org/10.1007/s00024-009-0495-0.
17. Paterson MS, Wong T-F. *Experimental Rock Deformation - the Brittle Field.* Berlin: Springer; 2005.
18. Guo H, Aziz NI, Schmidt LC. Rock fracture-toughness determination by the Brazilian test. *Eng Geol.* 1993;33(3):177–188. https://doi.org/10.1016/0013-7952(93)90056-I.
19. Groenenboom J, Van Dam DB. Monitoring hydraulic fracture growth: Laboratory experiments. *Geophysics.* 2000;65(11):603–611. https://doi.org/10.1190/1.1444756.
20. de Pater CJ, Weijers L, Savic M, Wolf KHAA, van den Hoek PJ, Barr DT. Experimental study of nonlinear effects in hydraulic fracture propagation(includes associated papers 29225 and 29687). *SPE Prod Facil.* 1994;9(04):239–246. https://doi.org/10.2118/25893-PA.
21. Madonna C, Almqvist BSG, Saenger EH. Digital rock physics: numerical prediction of pressure-dependent ultrasonic velocities using micro-CT imaging. *Geophys J Int.* 2012;189(3):1475–1482. https://doi.org/10.1111/j.1365-246X.2012.05437.x.
22. Krakowska P, Dohnalik M, Jarzyna J, Wawrzyniak-Guz K. Computed X-ray microtomography as the useful tool in petrophysics: a case study of tight carbonates modryn formation from Poland. *J Nat Gas Sci Eng.* 2016;31:67–75.
23. Saxena N, Hofmann R, Alpak FO, Dietderich J, Hunter S, Day-Stirrat RJ. Effect of image segmentation & voxel size on micro-CT computed effective transport & elastic properties. *Mar Petrol Geol.* 2017;86:972–990.
24. Alsayed MI. Utilising the Hoek triaxial cell for multiaxial testing of hollow rock cylinders. *Int J Rock Mech Min Sci.* 2002;39:355–366. https://doi.org/10.1016/S1365-1609(02)00030-8.
25. Bakker RR, Fazio M, Benson PM, Hess KU, Dingwell DB. The propagation and seismicity of dyke injection, new experimental evidence. *Geophys Res Lett.* 2016;43(5):1876–1883. https://doi.org/10.1002/2015GL066852.
26. Yang SQ. Experimental study on deformation, peak strength and crack damage behavior of hollow sandstone under conventional triaxial compression. *Eng Geol.* 2016;213:11–24. https://doi.org/10.1016/j.enggeo.2016.08.012.
27. Zoback MD, Moos D, Mastin L, Anderson RN. Well bore breakouts and in situ stress. *J. Geophys. Res. Solid Earth.* 2009;90:5523–5530.
28. Thomas N, Weijermars R. Comprehensive atlas of stress trajectory patterns and stress magnitudes around cylindrical holes in rock bodies for geoscientific and geotechnical applications. *Earth Sci Rev.* 2018. https://doi.org/10.1016/j.earscirev.2018.01.005.